Kinetic Evidence for Three Photolyzable Taxonomic Conformational Substates in Oxymyoglobin

Catherine Tetreau, Eugene Novikov, Martine Tourbez, and Daniel Lavalette
Institut Curie-Recherche (INSERM U350), Bâtiment 112, Centre Universitaire, 91405 Orsay, France

ABSTRACT The kinetics of oxygen geminate binding with the taxonomic substates of MbO_2 are reported. The maximum entropy method was used to analyze the rebinding kinetics of MbCO and MbO_2 monitored in the Soret. The resulting rate distributions were found to consist of a small number of overlapping bands. A global parametric fit of a series of rate distributions recorded at several temperatures was performed using a Gaussian basis set to resolve the individual enthalpy distributions $P(H)$. This approach was first validated by showing that the well-documented taxonomic substates of MbCO could be recovered. The method was then applied to MbO_2. Three taxonomic substates were identified at pH 4.8, whereas only two of them contribute to oxygen geminate rebinding at pH 7.0. These findings show that, similarly to MbCO, MbO_2 also exists as three photolyzable and kinetically different taxonomic substates and suggest reconsidering the issue of the photolysis quantum yield of MbO_2.

INTRODUCTION

The carbon monoxide complex of sperm whale myoglobin (sw MbCO) presents three well-documented taxonomic conformational substates A_0, A_1, and A_3 characterized by different CO stretch frequencies in the near infrared (Alben et al., 1982; Ansari et al., 1987). Their relative occupancy depends on a number of external parameters such as pH, temperature, pressure, and crystal form (Ansari et al., 1987; Iben et al., 1988; Frauenfelder et al., 1990; Hong et al., 1990; Müller et al., 1999). In the absence of conformational fluctuations, e.g., in hydro-organic solvents below 180 K, the taxonomic substates (CS^0) are frozen in a nonequilibrium distribution with invariant proportions. Flash photolysis experiments monitoring the CS^0 individually in the infrared band showed that the kinetics are nonexponential, indicating that each CS^0 consists of a wide distribution of CS^1 conformational substates (Ansari et al., 1987; Johnson et al., 1996). The overall CO rebinding rates decrease in the order $A_0 > A_1 > A_3$.

The taxonomic substates of MbO_2 are more difficult to characterize because the O—O stretch bands are intrinsically weak and appear in a spectral region in which absorbance of water, protein, and heme are predominant (Potter et al., 1987). In addition, the photolysis quantum yield of MbO_2 is significantly smaller than that of MbCO (Chance et al., 1990; Miller and Chance, 1995). As a consequence, nothing is known concerning the rebinding kinetics of O_2 with the taxonomic substates of MbO_2 individually.

In the present work we attempted to circumvent the difficulties associated with infrared kinetic spectroscopy of MbO_2. The electronic Soret absorption band in the visible is specific of the heme group and kinetic experiments monitored in this region measure the total amount of unbound ligand. It has been argued that such measurements do not distinguish among different taxonomic substates and yield information only about the average rebinding behavior (Johnson et al., 1996). In fact the Soret absorption band of the CS^0 are not exactly identical. Hole burning experiments with MbCO have shown that, compared with A_1, the Soret band of A_0 is shifted by 0.4 nm to the blue and that of A_3 by 0.6 nm to the red (Ormos et al., 1990). Thus, upon ligand photodissociation at low temperature, the transient absorption change in the Soret displays inhomogeneous kinetics corresponding to a superposition of the rebinding rate distribution of all CS^0.

We have reinvestigated the kinetics of geminate CO rebinding with Mb in the Soret using the maximum entropy method (MEM) to obtain the rate distribution $P(\log k)$ of the nonexponential kinetics between 77 and 170 K. These distributions indicate that several kinetic species are contributing to rebinding. A global analysis of the rate distributions provided evidence that these species may be assigned to the taxonomic conformational substates of MbCO. The method was then applied to oxygen geminate rebinding in MbO_2. We found that MbO_2 also exists in three different photolyzable CS^0, each of them being characterized by a phololysis yield smaller than unity.

MATERIALS AND METHODS

Materials

A sample of lyophilized sperm whale Mb (Serva, Heidelberg, Germany) that had been kept in liquid nitrogen was freshly purified by passage through a Sephadex G-75 column. The required amount of Mb was diluted with glycerol, buffer, and water to reach a final protein concentration of 10 to 20 μM in 50 mM buffer. Samples at pH 4.8 and 7.0 were prepared by using a potassium citrate/phosphate or a potassium phosphate buffer, respectively. (At low temperature the pH is expected to increase by $\sim$1 unit.) Experiments were performed in 79% (w/w) glycerol (glass transition

Submitted July 17, 2001, and accepted for publication December 13, 2001.
Address reprint requests to Dr. Daniel Lavalette, Institut Curie-Recherche (INSERM U350), Bâtiment 112, Centre Universitaire, 91405 Orsay, France. Tel.: 33-1-63-86-31-62; Fax: 33-1-69-07-53-27; E-mail: daniel.lavalette@curie.u-psud.fr

0006-3495/02/04/2148/08 $2.00

temperature $T_g \approx 173$ K). The ferrous CO complexes were prepared by passing a stream of CO above the protein solution submitted to gentle stirring, and adding a few microliters of a concentrated deaerated dithionite solution. The oxygenated complexes were prepared by passing a stream of argon above the solution and adding oxygen after reduction with sodium dithionite. Ligand binding was controlled by following the absorption change in the Soret.

Methods

Data collection

Sw Mb solutions in gas tight square cuvettes were cooled in a liquid nitrogen cryostat (Oxford Instruments DN704). Rebinding kinetics were recorded at 10- to 20-K intervals. The cooling rate was ~2 K/min, and the protein was allowed to equilibrate for further 15 min once the desired temperature was reached. Photodissociation was achieved by the 10-ns pulse of the second harmonic (532 nm) of a Q-switched Nd-YAG laser (Quantel, France). Transient absorption changes, monitored at the peak of the Soret band of the hexa-coordinated complex (423 nm for CO and 418 nm for O_2) or of the deoxy Mb (434 nm), were recorded over two decades in amplitude and six to seven decades in time using our fast kinetic spectrometer set-up (Tetreau et al., 1997).

Distribution of rate parameters and of activation enthalpy

Geminate rebinding is a first-order process. Due to the wide distribution of conformational substates (CS^1) in the rigid, glassy solvent, kinetics are highly nonexponential. The overall survival fraction $N(t)$ of unrecombined proteins is given by:

$$N(t) = \int_0^\infty P(\log k) e^{-kt} d(\log k) \qquad (1)$$

The rate distribution (or rate spectrum), $P(\log k)$, was obtained from the observed kinetics $N(t)$ by Laplace inversion of Eq. 1 using the MEM starting from a set of logarithmically spaced and equiprobable k values (Lavalette et al., 1991; Steinbach et al., 1991). This probability density function provides an equivalent description of the rebinding kinetics but is more powerful for analyzing complex processes.

Within one given taxonomic substate (CS^0), the rate distribution is caused by the distribution of the activation enthalpy $P(H, T)$ among CS^1, the preexponential factor A remaining sharp. Below the solvent's glass transition temperature, T_g, interconversion among CS does not take place, the protein ensemble is frozen, and the enthalpy distribution remains equal to $P(H, T_g)$ at any $T < T_g$. The enthalpy distribution is usually obtained by simple transformations from a set of $P(\log k)$ determined at different temperatures (Tetreau et al., 1997). Recent developments of our software now also permit to determine unimodal $P(H)$ by a global maximum entropy fit of a series of kinetics recorded at different temperatures. For multimodal $P(H)$, such as those observed in P450 (Tetreau et al., 1997) and in this work, this approach is not sufficient. Characterizing each mode (or subset) by an independent $\{A_i; P_i(H)\}$ pair is easy when the modes are well separated, but additional assumptions are needed when several $P(\log k)$ bands are overlapping and shift with respect to each other with temperature. In the absence of a theoretical model, we approximate the shape of the individual bands by a Gaussian. We consider the series of rate spectra $P(\log k)$ obtained at different temperatures below T_g as secondary data and perform a global parametric fit of all $P(\log k)$ by developing the enthalpy distribution:

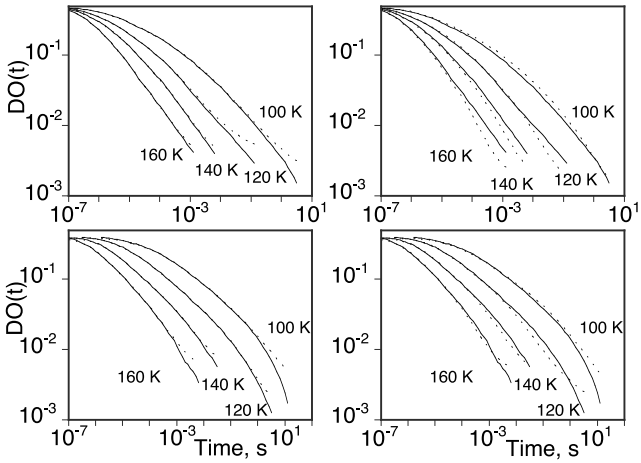

FIGURE 1 Examples of geminate rebinding kinetics (*full lines*) of MbCO at pH 4.8 (*top*) and 7.0 (*bottom*). (*Left*) MEM fits (*dotted lines*) corresponding to the MEM rate distributions of Figs. 2 and 3. (*Right*) Backward calculation (*dotted lines*) of the kinetics corresponding to the parametric global enthalpy fit of the rate spectra using a Gaussian model.

$$P(H) = \sum_1^3 \alpha_i G_i(H) \qquad (2)$$

in which the G_i are Gaussians with temperature independent mean and standard deviation. Their weighting factors α_i remain constant at all temperatures lower than T_g. Each G_i is associated with a preexponential factor A_i. The T-independent global $P(H)$ is linked to individual $P(\log k)$ by:

$$k = A(T/T_0) \exp(-H/RT) \qquad (3)$$

which yields the simple Arrhenius relation if T_0 is permanently equal to T. However, to compare our results with those of the literature, we used the transition state-like relation obtained by assigning to T_0 the constant value $T_0 = 100$ K (Dlott et al., 1983).

By definition the MEM yields the "optimum," or most likely, rate distribution corresponding to the experimental kinetics. Therefore, it is not surprising that the backward calculation of the kinetics by Laplace transformation of the Gaussian enthalpy model departed somewhat from the MEM fit, due to the approximation of the Gaussian bandshape. However, the overall agreement was generally quite satisfactory (Fig. 1). For this reason, we prefer to fit the rate spectra rather than using the approximate model of Eq. 2 to fit the kinetics directly.

Wide-band ultraviolet-visible monitoring

The more details are present in the rate spectra, the more accurate their decomposition into individual components will be. The rate profile was found to change with the monitoring wavelength as well as with the spectral bandwidth used, as expected for the inhomogeneous Soret. In addition, we observed that rate distributions tended to exhibit a more pronounced structure when the kinetics were recorded using a large spectral bandwidth. To see how kinetic information is recovered under condition of wide-band ultraviolet-visible monitoring, we first consider for simplicity an inhomogeneous absorption band resulting from the presence of only two species, P and Q, in the concentration ratio: c_p/c_q. Assuming

two kinetically distinct photoproducts, P^* and Q^*, the overall survival (rebinding) function is:

$$N(t) = c_{p^*}(0)n_{p^*}(t) + c_{q^*}(0)n_{q^*}(t) \quad (4)$$

in which $n_{p^*,\,q^*}(t)$ and $c_{p^*,\,q^*}(0)$ are the normalized survival probabilities and the initial concentrations of the photoproducts respectively. The latter depends on the ratio of the extinction coefficient ϵ_i of P and Q and of the photolysis quantum yield ϕ_i at the excitation wavelength. With monochromatic laser excitation:

$$c_{p^*}(0)/c_{q^*}(0) = (\phi_p\varepsilon_p c_p/\phi_q\varepsilon_q c_q)_{\lambda_e} \quad (5)$$

If the spectral width $\Delta\lambda$ of the monitoring light is relatively large (e.g. $\approx$ 10 nm or more), Beer-Lambert's law must be integrated over the whole spectral interval, yielding for the apparent transient absorbance change generated during rebinding:

$$\delta D_{app}(\Delta\lambda;\, t) = (\{\varepsilon_{p^*}\} - \{\varepsilon_p\})c_{p^*}(0)n_{p^*}(t) + (\{\varepsilon_{q^*}\} - \{\varepsilon_q\})c_{q^*}(0)n_{q^*}(t) \quad (6)$$

in which:

$$\{\varepsilon\} = \int I_0(\lambda)\varepsilon(\lambda)d\lambda \Big/ \int I_0(\lambda)d\lambda \quad (7)$$

is a function of the spectral intensity $I_o(\lambda)$ of the impinging light beam and of the decimal molar extinction coefficients $\epsilon_i(\lambda)$. If the wavelength dependence of $I_o(\lambda)$ can be neglected in the observation range $\Delta\lambda$ then $\{\epsilon\}$ becomes equal to $\langle\epsilon\rangle$, the average of the extinction coefficient over the wavelength interval. With monochromatic monitoring $\{\epsilon\} = \langle\epsilon\rangle = \epsilon$ and $\delta D_{app}(\Delta\lambda;\, t) = D(\lambda;\, t)$.

Eq. 6 indicates that the initial kinetic information is recovered except for a change of the amplitudes. This is not a limitation because in flash photolysis amplitudes are never directly representative of the concentration ratio of the species initially present (because of different yields and extinction coefficients).

In this work the detection system comprised a monochromator whose slits were adjusted to a fixed value corresponding to a spectral bandwidth $\Delta\lambda$ = 10 nm compared with the Soret one-half width of ~16 nm. The intensity of the monitoring light beam was maintained at the nominal value suitable for the photoreceptor by means of a variable neutral density filter. At low temperature, where rebinding is slow, pumping by the monitoring light may possibly represent another cause of distortion of the rate distribution because long-lived components will be predominantly affected. We therefore favored an observation in the Soret of the penta-coordinated (photodissociated heme) at 434 nm. In this way, illumination within the Soret of the dissociable hexa-coordinated was minimized by using a low pass, broadband interference filter.

RESULTS AND DISCUSSION

The kinetics of CO and O_2 rebinding with sw Mb were determined at low spectral resolution in the Soret absorption band of the deliganded (penta-coordinated heme) species at two different pH values. Although they were quite similar to those repeatedly reported in the literature by monitoring the Soret of the hexa-coordinated heme with monochromatic resolution (Austin et al., 1975; Doster et al., 1982; Steinbach et al., 1991; Johnson et al., 1996), subtle details could be appreciated only after computing the rate distributions. Rate distributions have been occasionally reported for Mb

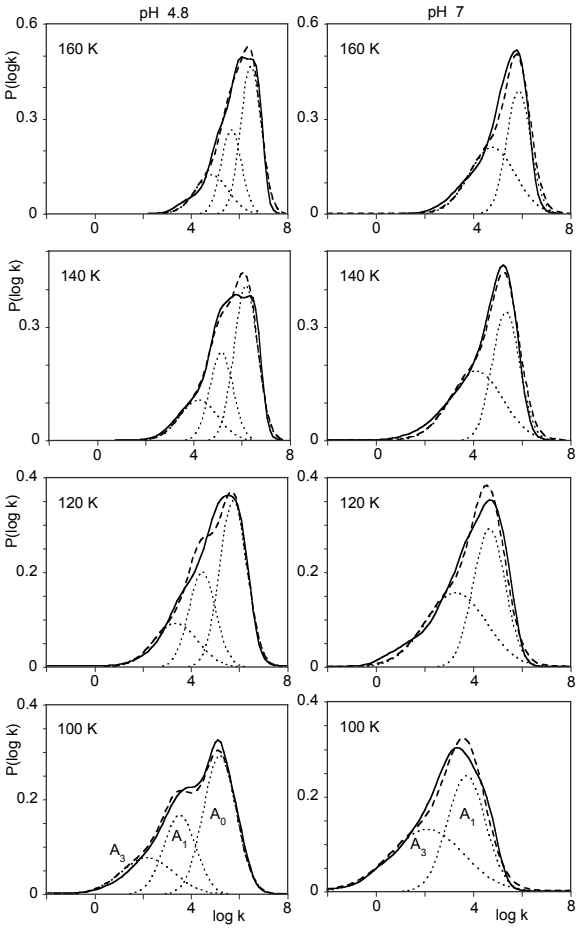

FIGURE 2 Rate distributions of geminate CO rebinding with sw Mb at pH 4.8 (*left*) and 7 (*right*) monitored at low spectral resolution in the Soret ($\Delta\lambda$ = 10 nm). Although the enthalpy distribution $P(H, T_g)$ is invariant, $P(\log k)$ broadens and shifts toward lower k values at low temperature because of the temperature dependence of k on H. The decomposition resulting from the global fit of the rate distribution according to the sum of Gaussian enthalpy distributions (Eq. 6) is shown in dotted lines with the proposed assignments to the CS^0. The contribution of each substate to the total signal can be evaluated from the integral under the curves. As explained in the text (Eqs. 2 and 3), they are not representative of the relative CS^0 probabilities.

(Steinbach et al., 1991, 1992; Lambright et al., 1993; Johnson et al., 1996), but no systematic MEM analysis covering the whole temperature range has been published. The rate distributions $P(\log k)$ are shown in Figs. 2 and 4. The irregular band shape suggests that several kinetic components are overlapping and that their contributions are redistributed between pH 4.8 and 7.

The analysis of the complex rate spectra depends on the reliability of the band shape recovered by the MEM. The principal advantage of the inversion of Eq. 1 by the MEM is that this method, contrary to parametric fitting, does not require postulating any analytical model. It yields the most general rate distribution that is consistent with inherently noisy data. An incorrect estimation of noise is therefore a

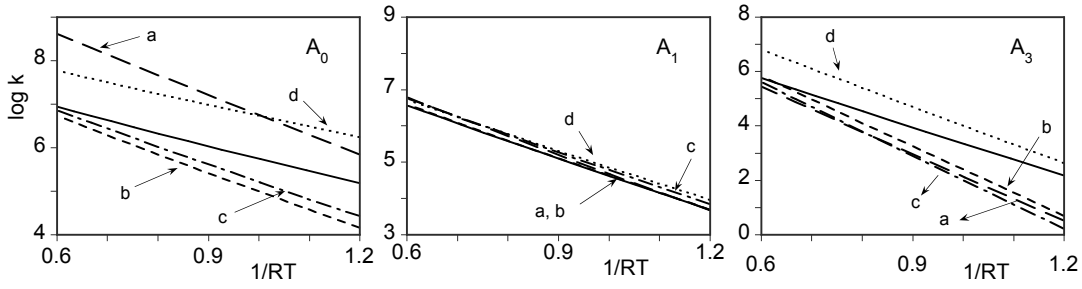

FIGURE 3 Arrhenius plots of k_{peak} of CO geminate rebinding with the taxonomic substates A_0, A_1, and A_3 of sw Mb calculated using data from this work (*full lines*) and published data (*a*, Berendzen and Braunstein, 1990; *b*, Steinbach et al., 1991; *c*, Johnson et al., 1996; *d*, Nienhaus et al., 1998).

potential source of difficulties. If the estimation is too low, noise may be partially fitted as signal. The rate spectrum may then over interpret the data by showing unnecessary details. If, on the contrary, the noise estimate is too high, genuine kinetic details may be blurred or lost. Although an automatic noise estimator of the signal immediately before photolysis is part of our data processing software we apply the precautionary rule according to which only those details in the rate spectra that persist after arbitrarily increasing twofold the noise values are considered as genuine. This ensures that the data will never be over interpreted. In this work, the reproducible effects of pH upon the band shape of the rate spectra further confirm that details in band profiles are significant.

CS^0 substates of sw MbCO

The rate distributions of MbCO (Fig. 2) could be fitted equally with a sum of two or three Gaussians, but doing so did not automatically warrant the temperature invariance of the enthalpy peak and width values nor that of their relative weight. Infrared monitoring indicates that only the relative populations of the taxonomic substates are affected by pH, whereas the rebinding enthalpy and preexponential factor of the individual CS^0 remain unchanged (Ansari et al., 1987; Mourant et al., 1993). We therefore performed a global fit of the rate distributions in which, at a given pH, all spectra were fitted assuming the same number of Gaussians under the constraint that their weighting factors remain constant at all temperatures.

In line with previous observations in the infrared bands indicating that only two CS^0 (A_1 and A_3) of MbCO have significant contributions at pH 7.0, whereas the contribution of A_0 becomes important at pH 4.8 (Ansari et al., 1987; Hong et al., 1990) we first fitted the rate distributions at pH 7 using a two-Gaussians model for the enthalpy distribution. This resulted in a satisfactory decomposition of the rate spectra, as shown in Fig. 2 (right). We then imposed the same H_i of the enthalpy bands obtained at pH 7 to fit the data at pH 4.8, leaving their relative weights as well as their preexponential factor free to vary. No satisfactory global fit could be obtained in this way. Only the addition of a third unconstrained Gaussian yielded the satisfactory decomposition shown in Fig. 2 (left). The data at pH 4.8 could be fitted with 3-Gaussian enthalpy bands as well without imposing the enthalpies derived from pH 7. The resulting enthalpy spectrum was very similar, except for some variation of the H_i compared with their values at pH 7. However, there is evidence from the literature for the invariance of the enthalpy with pH (Ansari et al., 1987; Mourant et al., 1993). Deviations may be expected with the choice of the fitting procedure, because a different question calls for a different answer. As we shall show below, the pH invariance was found to emerge naturally with MbO_2.

Within the experimental uncertainties, it can be concluded that three species are necessary to account for the rate distributions in the Soret of MbCO: they all appear at pH 4.8, whereas only two of them are present at pH 7. The enthalpy distributions $P(H, T_g)$ at pH 4.8 and 7 are displayed in Fig. 5. The preexponential factors and $P(H)$ parameters are compared in Table 1 with those obtained by monitoring each CS^0 individually in the infrared (Ansari et al., 1987; Berendzen and Braunstein, 1990; Steinbach et al., 1991; Johnson et al., 1996; Nienhaus et al., 1998). Despite some variability, agreement is good enough to provide evidence that the kinetic species resolved in the Soret indeed correspond to the three taxonomic substates of MbCO.

The difficulty in recovering precise parameters for the CS^0 even with direct monitoring in the infrared is probably due to spectral overlap and small absorbance. More generally, experimental uncertainties lead to apparent entropy-enthalpy compensation because preexponential factor and enthalpy are linked parameters (via Eq. 3). In addition, the mathematical approach varies with authors. Using an singular valve decomposition approach Hagen et al. (1996) attempted to account for kinetic differences exhibited by MbCO in glycerol and in a trehalose glass by fitting their global $P(H)$ obtained at pH 8.0 with three Gaussians of identical width.

To appreciate the variability of the data we consider the Arrhenius plot of k_{peak} values computed using the parameters reported by different authors (Fig. 3). Agreement is

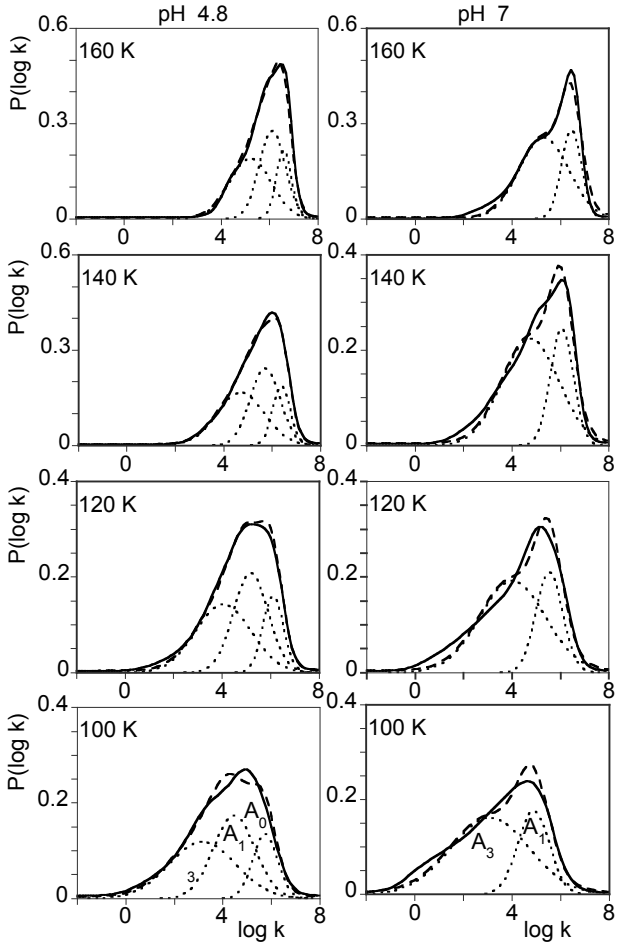

FIGURE 4 Rate distributions of geminate O_2 rebinding with sw Mb at pH 4.8 (*left*) and 7 (*right*) monitored at low spectral resolution in the Soret ($\Delta\lambda = 10$ nm). The decomposition resulting from the global fit of the rate distribution according to the sum of Gaussians enthalpy distribution (Eq. 6) is shown in dotted lines with the proposed assignments to the CS^0. Other remarks are as in Fig. 2.

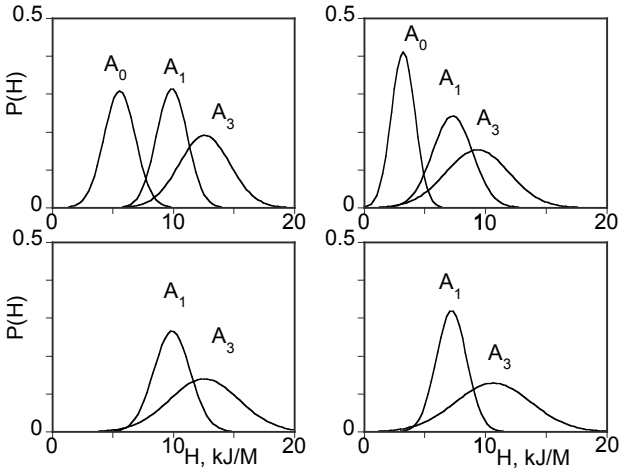

FIGURE 5 Normalized enthalpy distributions of the three CS° of sw MbCO (*left*) and sw MbO_2 (*right*) at pH 4.8 (*top*) and pH 7.0 (*bottom*).

excellent for A_1 but the parameters of the other taxonomic substates are more scattered, presumably in view of the experimental difficulties mentioned above. The present work yields results that are representative of the average among the determinations made by others.

Thus, although the present approach is indirect, its reliability is comparable with that of specific observations at the infrared wavelengths. Its main interest is to provide a straightforward alternative when infrared measurements are not possible, such as in the case of MbO_2 that we shall now examine.

CS^0 substates of sw MbO_2

Although their origin has long been debated, it is now commonly accepted that the taxonomic substates of liganded Mb are due to differences in the local electric field that result from alternative conformations of the distal histidine His-64. Their structure has been recently established at near atomic resolution (Vojtechovsky et al., 1999; Yang and Phillips, 1996). In MbCO, A_0 was identified with a doubly protonated histidine conformation, which is swung out of

TABLE 1 Thermodynamic parameters for CO rebinding with the CS° substates of sw Mb

References	log A (s^{-1})			H_{peak} (kJ/M)			Width (kJ/M)		
	A_0	A_1	A_3	A_0	A_1	A_3	A_0	A_1	A_3
This work (pH 4.8)	8.1	8.8	8.8	5.6	9.9	12.6	3.0	3.0	4.9
This work (pH 7.0)	—	8.9	8.7	—	9.9	12.6	—	1.5	2.9
Ansari et al., 1987	10.8	9.3	9.8	10.0	9.5	18.0	—	—	—
Berendzen and Braustein, 1990	10.8	9.3	9.8	9.5	10.8	17.8	11.0	7.0	9.0
Steinbach et al., 1991	8.7	8.9	10.4	8.7	10.0	18.6	6.0	7.0	9.0
Johnson et al., 1996	8.7	9.1	10.4	8.2	10.1	19.5	—	—	—
Nienhaus et al., 1998 (pH 5.1)*	8.7	8.9	10.4	4.7	9.1	13.8	6.3		
Nienhaus et al., 1998 (pH 7.0)*	8.7	8.9	10.4	3.1	9.5	14.9	6.3	8.4	10.8

The widths are the full widths measured at one-half maximum of the enthalpy distribution. Mean standard deviations are estimated as 0.8 for log A and 1.5 for H_{peak}.

*, Parameters of the main Gaussian components.

TABLE 2 Thermodynamic parameters for O_2 rebinding with the CS° substates of sw Mb

	log A (s^{-1})			H_p (kJ/M)			Width (kJ/M)		
References	A_0	A_1	A_3	A_0	A_1	A_3	A_0	A_1	A_3
This work, pH 4.8	7.4	8.3	8.1	3.2	7.3	9.4	2.3	3.9	6.1
This work, pH 7.0	—	8.6	8.6	—	7.2	10.7	—	2.9	7.3

The widths are the full widths measured at one-half maximum of the enthalpy distribution. Mean standard deviations are estimated as 0.8 for log A and 1.5 for H.

the pocket toward the solvent whereas A_1 and A_3 correspond to conformations of His-64 with N^ϵ pointing toward the heme and N^δ pointing out toward the solvent. They differ slightly in the distance between CO and N^ϵ. In MbO_2 only two conformations similar to those of the A_1 and A_3 substates of MbCO could be observed, the main difference being a hydrogen bond connecting the terminal oxygen atom with His-64-N^ϵ in A_3.

Because the structural features of the taxonomic substates of Mb imply essentially the protein and the protonation state of the distal histidine, one may reasonably expect to observe also the same CS^0 in MbO_2. Even though they are not spectroscopically resolvable in the infrared, their kinetic signature might be found by monitoring geminate rebinding in the Soret at low spectral resolution. The rate distributions for geminate oxygen binding and the decomposition resulting from a global fit using the Gaussian enthalpy model are presented in Fig. 4 and Table 2. Despite smaller signals, due to the reduced photolysis quantum yield of MbO_2, the structure of the rate distributions was slightly more pronounced than in MbCO. Again, three Gaussians were required to obtain good fits at pH 4.8, whereas only 2 were sufficient at pH 7.

Interestingly, the decomposition into three Gaussians at pH 4.8 gave almost identical results when H_1 and H_3 were fixed at the value derived from pH 7.0 or when they remained unconstrained. Therefore, the invariability of the enthalpy peaks with pH is more convincing with MbO_2.

The absence of A_0 in the crystal structure of sw MbO_2 at pH 6 is not clear. It might result from a smaller occupancy (<20%), a fact that might possibly point to some influence of the ligand upon the populations of the CS^0. The Soret kinetic data are consistent with three distinct taxonomic substates. An assignment to the A_1 and A_3 conformers modeling diffraction data appears inescapable at pH 7. One additional, faster rebinding CS^0 resembling closely A_0 of MbCO is found at pH 4.8.

Comparing Tables 1 and 2, it can be noted that, for a given ligand, the preexponential factors vary very little among the taxonomic substates, but that the prefactors of CO tend to exceed those of O_2 by a factor of ~3 (0.5 log units). The enthalpy spectrum for O_2 binding (Fig. 5) is rather close to that of CO after a global shift of 2.2 to 3.2 kJ/mol, toward low enthalpies, presumably because the naturally "bent" ligand experiences less steric hindrance. For both ligands, the peak enthalpies increase by ~4 kJ/mol between A_0 and A_1 and only by ~2.5 kJ/mol between A_1 and A_3. Again, this sequence is in agreement with the known ordering of the steric hindrance in the taxonomic substates.

To conclude this section, we believe that the evidence is strong enough that MbO_2, similarly to MbCO, may exist as three kinetically distinct taxonomic substates. With both ligands the activation enthalpy for binding can be regarded as being invariant upon a change of pH. Not only does sw MbO_2 appear to exist in the same CS^0 conformations as MbCO, but the fact that all of them are photolyzable sheds new light on the intriguing issue of the photodissociation quantum yield of oxygen.

Quantum yield of O_2 photolysis

The reason why, contrary to CO, the intrinsic quantum yield of O_2 photolysis appears smaller than unity (Chance et al., 1990) still remains a debated question. The difficulty with all reasoning about O_2 quantum yield may stem from the fact that it is often implicitly assumed that the photodissociation efficiency of one particular CS^0 can only be either 1 or 0. The present finding of three kinetic species implies that all CS^0 of MbO_2 are photolyzable, at least to some extent. (We wish to stress again that the amplitudes of the Gaussian components in the decomposition of $P(\log k)$ in Figs. 2 and 4 should not be used to estimate the relative quantum yields, as described by Eqs. 5 and 6. Thus the total quantum yield should be written in the general form:

$$\phi_T = \varphi_0 A_0 + \varphi_1 A_1 + \varphi_3 A_3 \quad (8)$$

in which A_i denotes the probability of the substates whose quantum yield φ_i may take any value between 0 and 1.

Another feature of MbO_2 is the pH dependence of the oxygen photolysis yield that decreases from ~0.5 at high pH to 0.1 to 0.2 at low pH (Miller et al., 1996). A detailed investigation of the pH dependence of the infrared CO stretch bands has shown that $A_1$and A_3 cannot be distinguished by a titration experiment because of an internal proton transfer that occurs without exchange with the solvent. Thus, $A^* = (A_1 + A_3)$ as a whole, is titrating against A_0. Moreover, the ratio $A_1/A_3 \approx 0.5$ remains nearly constant

over the whole pH range (Müller et al., 1999). Expressing Eq. 8 in terms of A^* and A_0, one obtains:

$$\phi = \varphi_0 + \frac{A^*}{A^* + A_0}[\alpha_1\varphi_1 + \alpha_3\varphi_3 - \varphi_0] \qquad (9)$$

in which the α_i are the fractions of $A_1$and A_3 constituting A^*.

Eq. 9 holds not only for sw Mb, but also for horse Mb in which A_3 is not observed. It is in agreement with the findings of Miller et al. (1996) who noticed that the pH dependence of the quantum yield of hh MbO_2 was following a tritration curve that parallels the pH-dependence of the A_0 subpopulation of MbCO.

Combining Eq. 9 with the above numerical data, one gets $\phi = (1/3)\varphi_1 + (2/3)\varphi_3 \approx 0.5$ and $\phi = \varphi_0 \approx 0.2$ at high and low pH respectively. Numerically, the first relation implies obviously that $\phi_3 < 1$ (in principle, no limit is obtained for ϕ_1). Whatever mechanism may be responsible for the low photoproduct yield of MbO_2, it appears that two CS^0 at least are affected, in contrast to the idea that just one of them would not be photolyzable.

It is very difficult to discuss the quantum yield issue in terms of high-resolution crystal structures of the taxonomic substates because these data concerns ligand-bound states only, whereas kinetic experiments monitor dissociated states, and quite obviously only those that live longer than the photolyzing flash. As noted by Chance et al. (1990) any dissociated state rebinding on a subpicosecond time scale would appear as "unphotolyzable."

The known crystallographic structure of photolysis intermediates in MbCO gives more relevant clues regarding the fate of the dissociated ligand. Immediately after photodissociation the ligand occupies a primary site above pyrole C at 3.6 Å from the heme (Schlichting et al., 1994; Hartmann et al., 1996; Chu et al., 2000). In the crystal, this species is trapped at temperatures below 40 K. At higher temperature, the ligand leaves the heme proximity to reach a new docking site, now identified with the distal xenon-binding site (Xe^4) (Ostermann et al., 2000). Other migration paths occur above 160 K (Chu et al., 2000; Ostermann et al., 2000), but between 40 and 160 K, geminate rebinding corresponds to the return of the ligand from the secondary (Xe^4) docking site. The quantum yields of MbCO taxonomic subtates are essentially unity, presumably because the relatively slow rebinding of this ligand cannot compete with escape toward (Xe^4).

Similar information is not available yet for the oxygen ligand, and the situation might be significantly different. If a primary docking site exists, its structure might not be related to that of CO, especially because O_2 can be involved in H bonding in many ways that might affect rebinding. (As an example, we may mention that the oxygenated complex of cytochrome P450cam, in which the oxygen ligand has been shown to take part in a H-bonding network (Schlichting et al., 2000) was found to be nonphotolyzable between 300 and 80 K (this laboratory, unpublished results). The fact that the photolysis yield of the oxygen CS^0 substates is smaller than unity removes some of the paradoxes that were pointed out previously (Vojtechovsky et al., 1999), but its understanding constitutes a new challenge requiring more information about the crystal structure of photolysis intermediates in MbO_2.

REFERENCES

Alben, J. O., D. Beece, S. F. Bowne, W. Doster, L. Eiseinstein, H. Frauenfelder, D. Good, J. D. McDonald, M. C. Marden, P. P. Moh, L. Reinisch, A. Reynolds, E. Shyamsunder, and K. T. Yue. 1982. Infrared spectroscopy of photodissociated carboxymyoglobin at low temperatures. *Proc. Natl. Acad. Sci. U. S. A.* 79:3744–3748.

Ansari, A., J. Berendzen, D. Braunstein, B. R. Cowen, H. Frauenfelder, M. K. Hong, I. E. T. Iben, J. B. Johnson, P. Ormos, T. B. Sauke, R. Scholl, A. Schulte, P. J. Steinbach, J. Vittitow, and R. D. Young. 1987. Rebinding and relaxation in the myoglobin pocket. *Biophys. Chem.* 26:337–355.

Austin, R. H., K. W. Beeson, L. Eisenstein, H. Frauenfelder, and I. C. Gunsalus. 1975. Dynamics of ligand binding to myoglobin. *Biochemistry.* 14:5355–5373.

Berendzen, J., and D. Braunstein. 1990. Temperature-derivative spectroscopy: a tool for protein dynamics. *Proc. Natl. Acad. Sci. U. S. A.* 87:1–5.

Chance, M. R., S. H. Courtney, M. D. Chavez, M. R. Ondrias, and J. M. Friedman. 1990. O_2 and CO reactions with heme proteins: quantum yields and geminate recombination on picosecond time scales. *Biochemistry.* 29:5537–5545.

Chu, K., J. Vojtechovsky, B. H. McMahon, R. M. Sweet, J. Berendzen, and I. Schlichting. 2000. Structure of a ligand-binding intermediate in wild-type carbonmonoxymyoglobin. *Nature.* 403:921–923.

Dlott, D. D., H. Frauenfelder, P. Langer, H. Roder, and E. E. DiIorio. 1983. Nanosecond flash photolysis study of carbon monoxide binding to the β chain of hemoglobin Zürich [β63(E7)His→Arg]. *Proc. Natl. Acad. Sci. U. S. A.* 80:6239–6243.

Doster, W., D. Beece, S. F. Bowne, E. E. DiIorio, L. Eisenstein, H. Frauenfelder, L. Reinisch, E. Shymsunder, K. H. Winterhalter, and K. T. Yue. 1982. Control and pH dependence of ligand binding to heme proteins. *Biochemistry.* 21:4831–4839.

Frauenfelder, H., N. A. Alberding, A. Ansari, D. Braunstein, B. R. Cowen, M. K. Hong, I. E. T. Iben, J. B. Johnson, S. Luck, J. R. Mourant, P. Ormos, L. Reinisch, R. Scholl, A. Schulte, E. Shyamsunder, L. B. Sorensen, P. J. Steinbach, A. Xie, R. D. Young, and K. T. Yue. 1990. Proteins and pressure. *J. Phys. Chem.* 94:1024–1038.

Hagen, S. J., J. Hofrichter, and W. A. Eaton. 1996. Geminate rebinding and conformational dynamics of myoglobin embedded in a glass at room temperature. *J. Phys. Chem.* 100:12008–12021.

Hartmann, H., S. Zinser, P. Komninos, R. T. Schneider, G. U. Nienhaus, and F. Parak. 1996. X-ray structure determination of a metastable state of carbonmonoxy myoglobin after photodissociation. *Proc. Natl. Acad. Sci. U. S. A.* 93:7013–7016.

Hong, M. K., D. Braunstein, B. R. Cowen, H. Frauenfelder, I. E. Iben, J. R. Mourant, P. Ormos, R. Scholl, A. Schulte, P. J. Steinbach, A.-H. Xie, and R. D. Young. 1990. Conformational substates and motions in myoglobin: external influences on structure and dynamics. *Biophys. J.* 58:429–436.

Iben, I. E. T., D. Braunstein, H. Frauenfelder, M. K. Hong, J. B. Johnson, S. Luck, P. Ormos, A. Schulte, P. J. Steinbach, A. H. Xie, R. D. Young, and W. Doster. 1988. Glassy behavior of a protein. *Phys. Rev. Lett.* 62:1916–1919.

Johnson, B. J., D. C. Lamb, H. Frauenfelder, J. D. Müller, B. McMahon, and G. U. Nienhaus. 1996. Ligand binding to heme proteins: VI. Interconversion of taxonomic substates in carbonmonoxymyoglobin. *Biophys. J.* 71:1563–1573.

Lambright, D. G., S. Balasubramanian, and S. G. Boxer. 1993. Dynamics of protein relaxation in site-specific mutants of human hemoglobin. *Biochemistry.* 32:10116–10124.

Lavalette, D., C. Tetreau, J.-C. Brochon, and A. Livesey. 1991. Conformational fluctuations and protein reactivity: determination of the rate-constant spectrum and consequences in elementary biochemical processes. *Eur. J. Biochem.* 196:591–598.

Miller, L. M., and M. R. Chance. 1995. Structural and electronic factors that influence oxygen affinities: a spectroscopic comparison of ferrous and cobaltous oxymyoglobin. *Biochemistry.* 34:10170–10179.

Miller, L. M., M. Patel, and M. R. Chance. 1996. Identification of conformational substates in oxymyoglobin through the pH dependence of the low temperature photoproduct yield. *J. Am. Chem. Soc.* 118:4511–4517.

Mourant, J. R., D. P. Braunstein, K. Chu, H. Frauenfelder, G. U. Nienhaus, P. Ormos, and R. D. Young. 1993. Ligand binding to heme proteins: II. Transitions in the heme pocket of myoglobin. *Biophys. J.* 65: 1496–1507.

Müller, J. D., B. H. McMahon, E. Y. T. Chien, S. G. Sligar, and G. U. Nienhaus. 1999. Connection between the taxonomic substates and protonation of histidines 64 and 97 in carbonmonoxy myoglobin. *Biophys. J.* 77:1036–1051.

Nienhaus, G. U., K. Chu, and K. Jesse. 1998. Structural heterogeneity and ligand binding in carbon monoxy myoglobin crystals at cryogenic temperatures. *Biochemistry.* 37:6819–6823.

Ormos, P., A. Ansari, D. Braunstein, B. R. Cowen, H. Frauenfelder, M. K. Hong, I. E. T. Iben, T. B. Sauke, P. J. Steinbach, and R. D. Young. 1990. Inhomogeneous broadening in spectral bands of carbonmonoxymyoglobin: the connection between spectral and functional heterogeneity. *Biophys. J.* 57:191–199.

Ostermann, A., R. Waschipky, F. G. Parak, and G. U. Nienhaus. 2000. Ligand binding and conformational motions in myoglobin. *Nature.* 404:205–208.

Potter, W. T., M. P. Tucker, R. A. Houtchens, and W. S. Caughey. 1987. Oxygen infrared spectra of oxyhemoglobins and oxymyoglobins: evidence of two major liganded O_2 structures. *Biochemistry.* 26: 4699–4707.

Schlichting, I., J. Berendzen, K. Chu, A. M. Stock, S. A. Maves, D. E. Benson, R. M. Sweet, D. Ringe, G. A. Petsko, and S. G. Sligar. 2000. The catalytic pathway of cytochrome P450cam at atomic resolution. *Science.* 287:1615–1622.

Schlichting, L., J. Berendzen, G. N. Phillips, Jr., and R. M. Sweet. 1994. Crystal structure of photolysed carbonmonoxy-myoglobin. *Nature.* 371: 808–812.

Steinbach, P. J., A. Ansari, J. Berendzen, D. Braunstein, K. Chu, B. R. Cowen, D. Ehrenstein, H. Frauenfelder, J. Bruce Johnson, D. C. Lamb, S. Luck, J. R. Mourant, G. U. Nienhaus, P. Ormos, R. Philipp, A. Xie, and R. D. Young. 1991. Ligand binding to heme proteins: connection between dynamics and function. *Biochemistry.* 30:3988–4001.

Steinbach, P. J., K. Chu, H. Frauenfelder, J. B. Johnson, D. C. Lamb, G. U. Nienhaus, T. B. Sauke, and R. D. Young. 1992. Determination of rate distributions from kinetic experiments. *Biophys. J.* 61:235–245.

Tetreau, C., C. Di Primo, R. Lange, H. Tourbez, and D. Lavalette. 1997. Dynamics of carbon monoxide binding with cytochromes P-450. *Biochemistry.* 36:10262–10275.

Vojtechovsky, J., K. Chu, J. Berendzen, R. M. Sweet, and L. Schlichting. 1999. Crystal structures of myoglobin-ligand complexes at near-atomic resolution. *Biophys. J.* 77:2153–2174.

Yang, F., and J. G. N. Phillips. 1996. Crystal structures of CO-, deoxy- and met-myoglobins at various pH values. *J. Mol. Biol.* 256:762–774.